Available online at www.sciencedirect.com
SCIENCE DIRECT®
Physics Letters B 553 (2003) 141–158
PHYSICS LETTERS B
www.elsevier.com/locate/npe

Observation of the strange sea in the proton via inclusive ϕ-meson production in neutral current deep inelastic scattering at HERA

ZEUS Collaboration

S. Chekanov, D. Krakauer, S. Magill, B. Musgrave, J. Repond, R. Yoshida

Argonne National Laboratory, Argonne, IL 60439-4815, USA [49]

M.C.K. Mattingly

Andrews University, Berrien Springs, MI 49104-0380, USA

P. Antonioli, G. Bari, M. Basile, L. Bellagamba, D. Boscherini, A. Bruni, G. Bruni, G. Cara Romeo, L. Cifarelli, F. Cindolo, A. Contin, M. Corradi, S. De Pasquale, P. Giusti, G. Iacobucci, A. Margotti, R. Nania, F. Palmonari, A. Pesci, G. Sartorelli, A. Zichichi

University and INFN Bologna, Bologna, Italy [40]

G. Aghuzumtsyan, D. Bartsch, I. Brock, S. Goers, H. Hartmann, E. Hilger, P. Irrgang, H.-P. Jakob, A. Kappes [1], U.F. Katz [1], O. Kind, E. Paul, J. Rautenberg [2], R. Renner, H. Schnurbusch, A. Stifutkin, J. Tandler, K.C. Voss, M. Wang, A. Weber

Physikalisches Institut der Universität Bonn, Bonn, Germany [37]

D.S. Bailey [3], N.H. Brook [3], J.E. Cole, B. Foster, G.P. Heath, H.F. Heath, S. Robins, E. Rodrigues [4], J. Scott, R.J. Tapper, M. Wing

H.H. Wills Physics Laboratory, University of Bristol, Bristol, United Kingdom [48]

M. Capua, A. Mastroberardino, M. Schioppa, G. Susinno

Calabria University, Physics Department and INFN, Cosenza, Italy [40]

J.Y. Kim, Y.K. Kim, J.H. Lee, I.T. Lim, M.Y. Pac [5]

Chonnam National University, Kwangju, South Korea [42]

doi:10.1016/S0370-2693(02)03206-9

A. Caldwell [6], M. Helbich, X. Liu, B. Mellado, Y. Ning, S. Paganis, Z. Ren, W.B. Schmidke, F. Sciulli

Nevis Laboratories, Columbia University, Irvington on Hudson, NY 10027, USA [50]

J. Chwastowski, A. Eskreys, J. Figiel, K. Olkiewicz, P. Stopa, L. Zawiejski

Institute of Nuclear Physics, Cracow, Poland [44]

L. Adamczyk, T. Bołd, I. Grabowska-Bołd, D. Kisielewska, A.M. Kowal, M. Kowal, T. Kowalski, M. Przybycień, L. Suszycki, D. Szuba, J. Szuba [7]

Faculty of Physics and Nuclear Techniques, University of Mining and Metallurgy, Cracow, Poland [51]

A. Kotański [8], W. Słomiński [9]

Department of Physics, Jagellonian University, Cracow, Poland

L.A.T. Bauerdick [10], U. Behrens, I. Bloch, K. Borras, V. Chiochia, D. Dannheim, M. Derrick [11], G. Drews, J. Fourletova, A. Fox-Murphy [12], U. Fricke, A. Geiser, F. Goebel [6], P. Göttlicher [13], O. Gutsche, T. Haas, W. Hain, G.F. Hartner, S. Hillert, U. Kötz, H. Kowalski [14], G. Kramberger, H. Labes, D. Lelas, B. Löhr, R. Mankel, I.-A. Melzer-Pellmann, M. Moritz [15], D. Notz, M.C. Petrucci [16], A. Polini, A. Raval, U. Schneekloth, F. Selonke [17], H. Wessoleck, R. Wichmann [18], G. Wolf, C. Youngman, W. Zeuner

Deutsches Elektronen-Synchrotron DESY, Hamburg, Germany

A. Lopez-Duran Viani [19], A. Meyer, S. Schlenstedt

DESY Zeuthen, Zeuthen, Germany

G. Barbagli, E. Gallo, C. Genta, P.G. Pelfer

University and INFN, Florence, Italy [40]

A. Bamberger, A. Benen, N. Coppola

Fakultät für Physik der Universität Freiburg i.Br., Freiburg i.Br., Germany [37]

M. Bell, P.J. Bussey, A.T. Doyle, C. Glasman, S. Hanlon, S.W. Lee, A. Lupi, G.J. McCance, D.H. Saxon, I.O. Skillicorn

Department of Physics and Astronomy, University of Glasgow, Glasgow, United Kingdom [48]

I. Gialas

Department of Engineering in Management and Finance, University of Aegean, Greece

B. Bodmann, T. Carli, U. Holm, K. Klimek, N. Krumnack, E. Lohrmann, M. Milite, H. Salehi, S. Stonjek [20], K. Wick, A. Ziegler, Ar. Ziegler

Hamburg University, Institute of Exp. Physics, Hamburg, Germany [37]

C. Collins-Tooth, C. Foudas, R. Gonçalo [4], K.R. Long, F. Metlica, A.D. Tapper

Imperial College London, High Energy Nuclear Physics Group, London, United Kingdom [48]

P. Cloth, D. Filges

Forschungszentrum Jülich, Institut für Kernphysik, Jülich, Germany

M. Kuze, K. Nagano, K. Tokushuku [21], S. Yamada, Y. Yamazaki

Institute of Particle and Nuclear Studies, KEK, Tsukuba, Japan [41]

A.N. Barakbaev, E.G. Boos, N.S. Pokrovskiy, B.O. Zhautykov

Institute of Physics and Technology of Ministry of Education and Science of Kazakhstan, Almaty, Kazakhstan

H. Lim, D. Son

Kyungpook National University, Taegu, South Korea [42]

F. Barreiro, O. González, L. Labarga, J. del Peso, I. Redondo [22], E. Tassi, J. Terrón, M. Vázquez

Departamento de Física Teórica, Universidad Autónoma de Madrid, Madrid, Spain [47]

M. Barbi, A. Bertolin, F. Corriveau, A. Ochs, S. Padhi, D.G. Stairs, M. St-Laurent

Department of Physics, McGill University, Montréal, QC, H3A 2T8 Canada [36]

T. Tsurugai

Meiji Gakuin University, Faculty of General Education, Yokohama, Japan

A. Antonov, P. Danilov, B.A. Dolgoshein, D. Gladkov, V. Sosnovtsev, S. Suchkov

Moscow Engineering Physics Institute, Moscow, Russia [45]

R.K. Dementiev, P.F. Ermolov, Yu.A. Golubkov, I.I. Katkov, L.A. Khein, I.A. Korzhavina, V.A. Kuzmin, B.B. Levchenko, O.Yu. Lukina, A.S. Proskuryakov, L.M. Shcheglova, N.N. Vlasov, S.A. Zotkin

Moscow State University, Institute of Nuclear Physics, Moscow, Russia [46]

C. Bokel, J. Engelen, S. Grijpink, E. Koffeman, P. Kooijman, E. Maddox, A. Pellegrino, S. Schagen, H. Tiecke, N. Tuning, J.J. Velthuis, L. Wiggers, E. de Wolf

NIKHEF and University of Amsterdam, Amsterdam, Netherlands [43]

N. Brümmer, B. Bylsma, L.S. Durkin, T.Y. Ling

Physics Department, Ohio State University, Columbus, OH 43210, USA [49]

S. Boogert, A.M. Cooper-Sarkar, R.C.E. Devenish, J. Ferrando, G. Grzelak, T. Matsushita, M. Rigby, O. Ruske [23], M.R. Sutton, R. Walczak

Department of Physics, University of Oxford, Oxford, United Kingdom [48]

R. Brugnera, R. Carlin, F. Dal Corso, S. Dusini, A. Garfagnini, S. Limentani, A. Longhin, A. Parenti, M. Posocco, L. Stanco, M. Turcato

Dipartimento di Fisica dell' Università and INFN, Padova, Italy [40]

E.A. Heaphy, B.Y. Oh, P.R.B. Saull [24], J.J. Whitmore [25]

Department of Physics, Pennsylvania State University, University Park, PA 16802, USA [50]

Y. Iga

Polytechnic University, Sagamihara, Japan [41]

G. D'Agostini, G. Marini, A. Nigro

Dipartimento di Fisica, Università 'La Sapienza' and INFN, Rome, Italy [40]

C. Cormack [26], J.C. Hart, N.A. McCubbin

Rutherford Appleton Laboratory, Chilton, Didcot, Oxon, United Kingdom [48]

C. Heusch

University of California, Santa Cruz, CA 95064, USA [49]

I.H. Park

Department of Physics, Ewha Womans University, Seoul, South Korea

N. Pavel

Fachbereich Physik der Universität-Gesamthochschule Siegen, Germany

H. Abramowicz, A. Gabareen, S. Kananov, A. Kreisel, A. Levy

Raymond and Beverly Sackler Faculty of Exact Sciences, School of Physics, Tel-Aviv University, Tel-Aviv, Israel [39]

T. Abe, T. Fusayasu, S. Kagawa, T. Kohno, T. Tawara, T. Yamashita

Department of Physics, University of Tokyo, Tokyo, Japan [41]

R. Hamatsu, T. Hirose [17], M. Inuzuka, S. Kitamura [27], K. Matsuzawa, T. Nishimura

Tokyo Metropolitan University, Deptartment of Physics, Tokyo, Japan [41]

M. Arneodo [28], M.I. Ferrero, V. Monaco, M. Ruspa, R. Sacchi, A. Solano

Università di Torino, Dipartimento di Fisica Sperimentale and INFN, Torino, Italy [40]

R. Galea, T. Koop, G.M. Levman, J.F. Martin, A. Mirea, A. Sabetfakhri

Department of Physics, University of Toronto, Toronto, ON, M5S 1A7 Canada [36]

J.M. Butterworth, C. Gwenlan, R. Hall-Wilton, T.W. Jones, M.S. Lightwood, J.H. Loizides [29], B.J. West

Physics and Astronomy Department, University College London, London, United Kingdom [48]

J. Ciborowski [30], R. Ciesielski [31], R.J. Nowak, J.M. Pawlak, B. Smalska [32], J. Sztuk [33], T. Tymieniecka [34], A. Ukleja [34], J. Ukleja, A.F. Żarnecki

Warsaw University, Institute of Experimental Physics, Warsaw, Poland [52]

M. Adamus, P. Plucinski

Institute for Nuclear Studies, Warsaw, Poland [52]

Y. Eisenberg, L.K. Gladilin [35], D. Hochman, U. Karshon

Department of Particle Physics, Weizmann Institute, Rehovot, Israel [38]

D. Kçira, S. Lammers, L. Li, D.D. Reeder, A.A. Savin, W.H. Smith

Department of Physics, University of Wisconsin, Madison, WI 53706, USA [49]

A. Deshpande, S. Dhawan, V.W. Hughes, P.B. Straub

Department of Physics, Yale University, New Haven, CT 06520-8121, USA [49]

S. Bhadra, C.D. Catterall, S. Fourletov, S. Menary, M. Soares, J. Standage

Department of Physics, York University, Ontario, M3J 1P3 Canada [36]

Received 7 November 2002; accepted 12 December 2002
Editor: W.-D. Schlatter

Abstract

Inclusive $\phi(1020)$-meson production in neutral current deep inelastic e^+p scattering has been measured with the ZEUS detector at HERA using an integrated luminosity of 45 pb^{-1}. The ϕ mesons were studied in the range $10 < Q^2 < 100$ GeV^2, where Q^2 is the virtuality of the exchanged photon, and in restricted kinematic regions in the transverse momentum, p_T, pseudorapidity, η, and the scaled momentum in the Breit frame, x_p. Monte Carlo models with the strangeness-suppression factor as determined by analyses of e^+e^- annihilation events overestimate the cross sections. A smaller value of the strangeness-suppression factor reduces the predicted cross sections, but fails to reproduce the shapes of the measured differential cross sections. High-momentum ϕ mesons in the current region of the Breit frame give the first direct evidence for the strange sea in the proton at low x.

E-mail address: b.foster@bristol.ac.uk (B. Foster).

[1] On leave of absence at University of Erlangen-Nürnberg, Germany.

[2] Supported by the GIF, contract I-523-13.7/97.

[3] PPARC Advanced fellow.

[4] Supported by the Portuguese Foundation for Science and Technology (FCT).

[5] Now at Dongshin University, Naju, Korea.

[6] Now at Max-Planck-Institut für Physik, München, Germany.

[7] Partly supported by the Israel Science Foundation and the Israel Ministry of Science.

[8] Supported by the Polish State Committee for Scientific Research, grant No. 2 P03B 09322.

[9] Member of Department of Computer Science.

[10] Now at Fermilab, Batavia, IL, USA.

[11] On leave from Argonne National Laboratory, USA.

[12] Now at R.E. Austin Ltd., Colchester, UK.

[13] Now at DESY group FEB.

[14] On leave of absence at Columbia Univ., Nevis Labs., NY, USA.

[15] Now at CERN.

[16] Now at INFN Perugia, Perugia, Italy.

[17] Retired.

[18] Now at Mobilcom AG, Rendsburg-Büdelsdorf, Germany.

[19] Now at Deutsche Börse Systems AG, Frankfurt/Main, Germany.

[20] Now at University of Oxford, Oxford, UK.

[21] Also at University of Tokyo.

[22] Now at LPNHE Ecole Polytechnique, Paris, France.

[23] Now at IBM Global Services, Frankfurt/Main, Germany.

[24] Now at National Research Council, Ottawa, Canada.

[25] On leave of absence at The National Science Foundation, Arlington, VA, USA.

[26] Now at University of London, Queen Mary College, London, UK.

[27] Present address: Tokyo Metropolitan University of Health Sciences, Tokyo 116-8551, Japan.

[28] Also at Università del Piemonte Orientale, Novara, Italy.

[29] Supported by Argonne National Laboratory, USA.

[30] Also at Łódź University, Poland.

[31] Supported by the Polish State Committee for Scientific Research, grant No. 2 P03B 07222.

[32] Now at The Boston Consulting Group, Warsaw, Poland.

[33] Łódź University, Poland.

[34] Supported by German Federal Ministry for Education and Research (BMBF), POL 01/043.

[35] On leave from MSU, partly supported by University of Wisconsin via the US–Israel BSF.

[36] Supported by the Natural Sciences and Engineering Research Council of Canada (NSERC).

[37] Supported by the German Federal Ministry for Education and Research (BMBF), under contract numbers HZ1GUA 2, HZ1GUB 0, HZ1PDA 5, HZ1VFA 5.

[38] Supported by the MINERVA Gesellschaft für Forschung GmbH, the Israel Science Foundation, the US–Israel Binational Science Foundation and the Benozyio Center for High Energy Physics.

[39] Supported by the German–Israeli Foundation and the Israel Science Foundation.

[40] Supported by the Italian National Institute for Nuclear Physics (INFN).

[41] Supported by the Japanese Ministry of Education, Science and Culture (the Monbusho) and its grants for Scientific Research.

[42] Supported by the Korean Ministry of Education and Korea Science and Engineering Foundation.

[43] Supported by the Netherlands Foundation for Research on Matter (FOM).

[44] Supported by the Polish State Committee for Scientific Research, grant No. 620/E-77/SPUB-M/DESY/P-03/DZ 247/2000-2002.

1. Introduction

The total quark content of the proton has been well determined [1–4] through analyses of inclusive deep inelastic scattering (DIS) data. However, the flavour decomposition of the sea is less well known. So far, experimental constraints on the strange-quark content of the nucleon have come from fixed-target neutrino experiments [5], which indicate that the $s\bar{s}$ is suppressed with respect to the $u\bar{u}$ and $d\bar{d}$ sea by a factor of about two. This paper reports a study of the production of ϕ-mesons in neutral current e^+p DIS and explores its sensitivity to the strange sea of the proton at low x.

Several mechanisms lead to ϕ-meson production in DIS. The ϕ meson, which is a nearly pure $s\bar{s}$ state, can be produced by the hadronisation of a strange quark created in the hard scattering process of a virtual photon on the strange sea of the proton, $\gamma^* s \to s$, as illustrated in Fig. 1(a). The underlying hard-scattering process is either zeroth order in QCD, namely the quark–parton model (QPM), or first order, $\gamma^* s \to sg$, the QCD Compton reaction (QCDC). Another source of strange quarks is boson–gluon fusion (BGF), $\gamma^* g \to s\bar{s}$, Fig. 1(b). In contrast to the QPM and QCDC processes, the rate of BGF events is related to the density of gluons in the proton and is, therefore, not directly dependent on the intrinsic sea-quark content of the proton. The hadronisation process alone, without strange quarks being involved in the hard scattering, contributes to the production

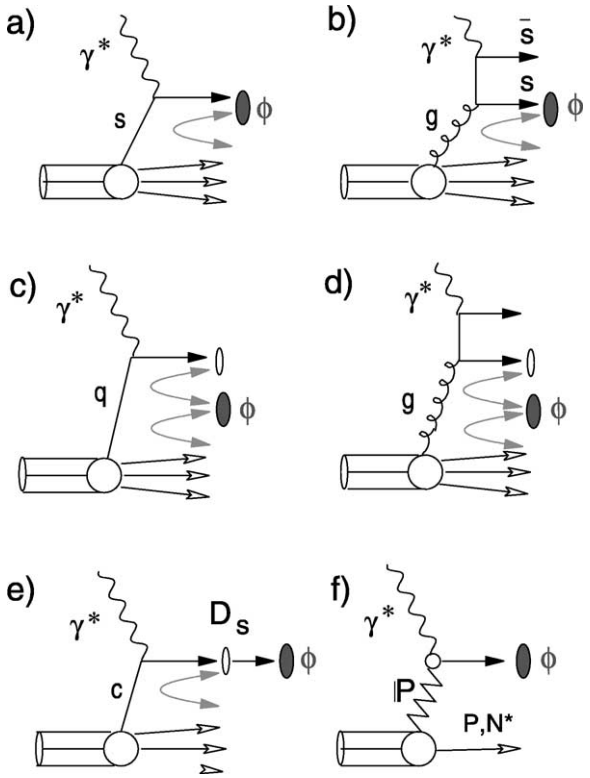

Fig. 1. A schematic representation of different mechanisms for ϕ production in inclusive DIS: (a) a ϕ meson is produced from a strange quark after the interaction on the strange sea according to the QPM; (b) a ϕ meson is produced from a strange quark emerging from the BGF process; (c), (d) a ϕ meson is produced solely by the hadronisation process, independent of the flavour of the quark participating in the hard interaction. Additional sources of ϕ mesons are the hadronisation of strange quarks produced by higher-order gluon splittings, resonance decays, such as (e) the D_s-meson decays; and (f) diffractive ϕ-meson production.

of ϕ mesons, as shown in Fig. 1(c), (d). In this case, ϕ mesons are formed from strange quarks created during hadronisation. Hadronisation of strange quarks produced in higher-order QCD reactions related to the splitting of gluons, $g \to s\bar{s}$, and the decay of higher-mass states, such as the D_s meson (Fig. 1(e)), also contribute. In addition, diffractive scattering can produce ϕ mesons in the final state (Fig. 1(f)).

Strange-particle production in inclusive DIS has been studied at HERA using K^0 mesons and Λ baryons [6,7]. However, their production rates are dominated by the fragmentation process and by the decays of high-mass states, and are, therefore, insensi-

[45] Partially supported by the German Federal Ministry for Education and Research (BMBF).

[46] Supported by the Fund for Fundamental Research of Russian Ministry for Science and Education and by the German Federal Ministry for Education and Research (BMBF).

[47] Supported by the Spanish Ministry of Education and Science through funds provided by CICYT.

[48] Supported by the Particle Physics and Astronomy Research Council, UK.

[49] Supported by the US Department of Energy.

[50] Supported by the US National Science Foundation.

[51] Supported by the Polish State Committee for Scientific Research, grant No. 112/E-356/SPUB-M/DESY/P-03/DZ 301/2000-2002, 2 P03B 13922.

[52] Supported by the Polish State Committee for Scientific Research, grant No. 115/E-343/SPUB-M/DESY/P-03/DZ 121/2001-2002, 2 P03B 07022.

tive to the presence of strange quarks in the hard scattering process. For ϕ mesons, the contribution from resonance decays is relatively small. Furthermore, selecting ϕ mesons with large longitudinal momenta in the Breit frame [8] enhances the contribution from the QPM process of Fig. 1(a).

In this study, the ϕ mesons were identified through the decay $\phi \to K^+K^-$. Their differential cross sections are presented as functions of $Q^2 = -q^2 = -(k-k')^2$ and Bjorken $x = Q^2/(2Pq)$, where k and k' are the four-momenta of the initial and scattered lepton and P is the four-momentum of the incoming proton, as well as other variables that characterise the ϕ-meson production.

2. Properties of ϕ mesons in the Breit frame

The Breit frame [8] provides a natural system to separate the radiation of the outgoing struck quark from the proton remnant. In this frame, the exchanged virtual boson with virtuality Q is space-like and has a momentum $q = (q_0, q_{X_B}, q_{Y_B}, q_{Z_B}) = (0, 0, 0, -Q)$. In the QPM, the incident quark has $p_{Z_B} = Q/2$ and the outgoing struck quark carries $p_{Z_B} = -Q/2$. All particles with negative p_{Z_B} form the current region. These particles are produced by the fragmentation of the struck quark, so that this region is analogous to a single hemisphere of an e^+e^- annihilation event.

The ϕ-meson cross sections are presented as a function of the scaled momentum, $x_p = 2p/Q$, where p is the absolute momentum of the ϕ meson in the Breit frame. In the QPM process, $\gamma^* s \to s$, this variable is equal to unity for the s-quarks in the current region. As a consequence, leading ϕ mesons in the current region with x_p values close to unity are a measure of the hard scattering of a virtual photon on the strange sea. Gluon radiation and the fragmentation process generally lead to particles with $x_p < 1$, and, much less frequently, to $x_p > 1$.

In the target region, x_p can be significantly larger than unity. This is because the maximum momentum of the proton remnant in the QPM is $Q(1-x)/2x$, therefore $x_p^{\max} = (1-x)/x$. The ϕ mesons in the target region are mostly produced by the hadronisation processes of Fig. 1(c), (d), as well as the hadronisation of strange quarks from the BGF diagram of Fig. 1(b).

3. Data sample and analysis procedure

3.1. Experimental setup

During the 1995–1997 period, 45.0 ± 0.7 pb^{-1} of data were taken with the ZEUS detector with a positron beam energy of 27.5 GeV and a proton beam energy of 820 GeV.

ZEUS is a multipurpose detector described in detail elsewhere [9]. Of particular importance in the present study are the central tracking detector and the calorimeter.

The central tracking detector (CTD) [10] is a cylindrical drift chamber with nine superlayers covering the polar-angle[53] region $15° < \theta < 164°$ and the radial range 18.2–79.4 cm. Each superlayer consists of eight sense-wire layers. The transverse-momentum resolution for charged tracks traversing all CTD layers is $\sigma(p_T)/p_T = 0.0058 p_T \oplus 0.0065 \oplus 0.0014/p_T$, with p_T in GeV.

The CTD is surrounded by the uranium-scintillator calorimeter, CAL [11], which is divided into three parts: forward, barrel and rear. The calorimeter is longitudinally segmented into electromagnetic and hadronic sections. The smallest subdivision of the CAL is called a cell. The energy resolution of the calorimeter under test-beam conditions is $\sigma_E/E = 0.18/\sqrt{E}$ for electrons and $\sigma_E/E = 0.35/\sqrt{E}$ for hadrons (with E in GeV).

The position of positrons scattered at small angles to the positron beam direction was measured using the small-angle rear tracking detector (SRTD) [12,13]. The energy of the scattered positrons was corrected for the energy loss in the material between the interaction point and the calorimeter using a presampler (PRES) [13,14].

[53] The ZEUS coordinate system is a right-handed Cartesian system, with the Z axis pointing in the proton beam direction, referred to as the "forward direction", and the X axis pointing left towards the centre of HERA. The coordinate origin is at the nominal interaction point. The pseudorapidity is defined as $\eta = -\ln(\tan\frac{\theta}{2})$, where the polar angle, θ, is measured with respect to the proton beam direction.

3.2. Kinematic reconstruction and event selection

The scattered-positron candidate was identified from the pattern of energy deposits in the CAL [15]. The kinematic variables, Q^2 and x, were reconstructed by the following methods:

- the electron method (this method is denoted by the subscript e) uses measurements of the energy and angle of the scattered positron;
- the double angle (DA) method [16] relies on the angles of the scattered positron and of the hadronic energy flow;
- the Jacquet–Blondel (JB) method [17] is based entirely on measurements of the hadronic system.

The DIS event selection was based on the following requirements:

- $E_{e'} \geqslant 10$ GeV, where $E_{e'}$ is the energy of the scattered positron in the calorimeter after the correction by the PRES;
- $10 < Q_e^2 < 100$ GeV^2. The upper cut on Q_e^2 was used to reduce the combinatorial background in the ϕ-meson reconstruction;
- $40 < \delta < 60$ GeV, where $\delta = \sum E_i(1 - \cos\theta_i)$, E_i is the energy of the ith calorimeter cell, θ_i is its angle, and the sum runs over all cells. This cut further reduces the background from photoproduction and events with large initial-state radiation;
- $y_e \leqslant 0.95$, to remove events with fake scattered positrons;
- $y_{\mathrm{JB}} \geqslant 0.04$, to improve the accuracy of the DA reconstruction used in systematic checks;
- a primary vertex position, determined from the tracks fitted to the vertex, in the range $|Z_{\mathrm{vertex}}| < 50$ cm, to reduce background events from non-ep interactions;
- the impact point (X, Y) of the scattered positron in the calorimeter must be within a radius $\sqrt{X^2 + Y^2} > 25$ cm.

The reconstruction of the Breit frame and the Q^2 and x variables was performed using the electron method, since it has the best resolution at the relatively low Q^2 values of this data set.

4. Selection of ϕ candidates

Charged tracks measured by the CTD and assigned to the primary event vertex were selected. Tracks were required to pass through at least three CTD superlayers and have transverse momenta $p_T > 200$ MeV in the laboratory frame, thus restricting the study to a CTD region where track acceptance and resolution are high.

All pairs of oppositely charged tracks were combined to form the ϕ candidates. The tracks were assigned the mass of a charged kaon when calculating the invariant mass, $M(K^+K^-)$, of each track pair. The events with ϕ-meson candidates were selected using the following requirements:

- $0.99 < M(K^+K^-) < 1.06$ GeV;
- $p_T^{\phi} > 1.7$ GeV and $-1.7 < \eta^{\phi} < 1.6$, where p_T^{ϕ} is the transverse momentum and η^{ϕ} is the pseudorapidity of the ϕ meson in the laboratory frame.

The asymmetric cut on η^{ϕ} was used to avoid the very forward region that has large track multiplicities, resulting in high combinatorial backgrounds.

Fig. 2(a) shows the invariant-mass distribution for ϕ candidates in the range $10 < Q^2 < 100$ GeV^2. The invariant mass for the leading ϕ mesons in the current region of the Breit frame, $0.8 < x_p < 1.1$, is presented in Fig. 2(b). For the latter case, the DIS events containing the ϕ-meson candidates have $x < 0.006$. The solid line in each figure is a fit using a relativistic Breit–Wigner (BW) function convoluted with a Gaussian distribution plus a term describing the background:

$$F(M) = (\mathrm{BW}) \otimes (\mathrm{Gaussian}) + a(M - 2m_K)^b,$$

where a and b are free parameters and m_K is the kaon mass. The fit function contains five free parameters: normalisation, peak position, width of the Gaussian distribution, and two parameters describing the background. When the peak position was left free, the resulting fit gave 1019.2 ± 0.3 MeV, in agreement with the PDG value of 1019.456 ± 0.020 MeV [18]. The width of the Gaussian was 1.6 ± 0.3 MeV, consistent with the tracking resolution. In order to improve the stability of the fit for the calculations of the differential cross sections, the mass peak and width of the Breit–Wigner function were fixed at the PDG values [18].

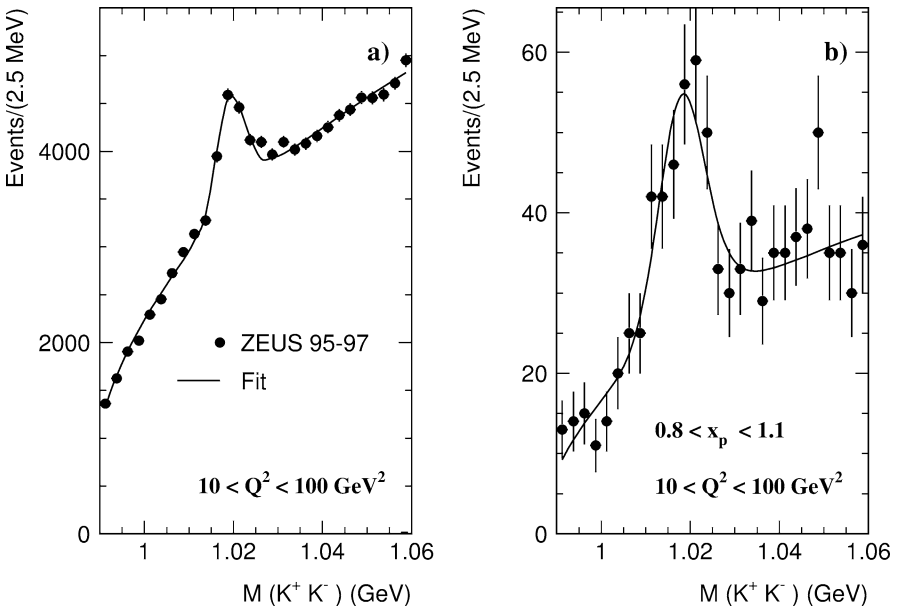

Fig. 2. The invariant mass of the ϕ-meson candidates (points with statistical error bars) (a) in the restricted kinematic regions $p_T^{\phi} > 1.7$ GeV and $-1.7 < \eta^{\phi} < 1.6$; (b) for the highest x_p value in the current region of the Breit frame, in addition to the cuts as in (a). The solid lines show the results of the fit described in the text.

The total number of ϕ-meson candidates determined from this fit was 4950 ± 214, while the number of ϕ-meson candidates for the high x_p region was 181 ± 28.

5. Event simulations

A good understanding of hadronisation is a prerequisite for the interpretation of the measured inclusive ϕ-meson cross sections. At present, only Monte Carlo (MC) models based on leading-order QCD are available to compare with the experimental results, so that the predictions for the rates of $s\bar{s}$ production are plagued by large model-dependent uncertainties. In MC models based on the Lund string fragmentation [19], the production ratio of strange to light non-strange quarks is parameterised by the strangeness-suppression factor, $\lambda_s = P_s/P_{u,d}$, where P_s ($P_{u,d}$) is the probability of creating s (u, d) quarks in the colour field during fragmentation. The processes shown in Fig. 1(a) and (b) are proportional to λ_s, while the contributions illustrated in Fig. 1(c) and (d) are proportional to λ_s^2.

In e^+e^- annihilation, the production of ϕ-mesons has been well described using $\lambda_s = 0.3$ [20]. However, there are new indications that a larger value, $\lambda_s \simeq 0.4$, may be needed [21], or even that a single value cannot accommodate all of the SLD strangeness-production data [22]. When using the same hadronisation model in e^+p scattering, the measured K^0 and Λ production rates in DIS [6,7] and photoproduction [23] indicate the need for a smaller value, $\lambda_s \simeq 0.2$.

The measured cross sections were compared to various leading-order MC models based on the QCD parton-cascade approach, to incorporate higher-order QCD effects, followed by fragmentation into hadrons. The MC events were generated with LEPTO 6.5 [24], ARIADNE 4.07 [25] and HERWIG 6.2 [26] using the default parameters in each case. The fragmentation in LEPTO and ARIADNE is simulated using the Lund string model [19] as implemented in PYTHIA [27], whereas the hadronisation stage in HERWIG is described by a cluster fragmentation model [28].

The acceptance was calculated using ARIADNE, which was interfaced with HERACLES 4.5.2 [29] using the DJANGOH program [30] in order to incorpo-

rate first-order electroweak corrections. The generated events were then passed through a full simulation of the detector using GEANT 3.13 [31] and processed with the same reconstruction program as used for the data. The detector-level MC samples were then selected in the same way as the data.

The natural width of the Breit–Wigner distribution for ϕ-meson decays was set to the default value [18] in LEPTO and ARIADNE. The HERWIG model sets the particle-decay width to zero and is therefore less realistic for the acceptance calculations. The HERWIG model was used only for comparisons with the final cross sections.

The inclusive ϕ-meson sample contains a contribution from diffractive processes, which is not well simulated in the MC models mentioned above. These processes are characterised by a rapidity gap, chosen as $\eta_{\max} < 2$, where $\eta_{\max}$ is defined as the pseudorapidity of the energy deposit in the CAL above 400 MeV closest to the proton direction, and by the presence in the CTD of only a few tracks. Diffractive events with ϕ mesons were generated with PYTHIA 5.7 [27] and passed through the same simulation of the detector as for inclusive MC events. The MC distributions were fit to the data by varying the fraction of the diffractive ϕ-meson events from PYTHIA and minimising the χ^2 to obtain good agreement for the multiplicity of charged tracks in the CTD. The fraction of PYTHIA events needed to obtain good agreement between data and MC was $2.7 \pm 0.2\%$ of the total number of reconstructed ϕ-meson events. It was verified that this fraction gives a satisfactory description of the ϕ-meson events for $\eta_{\max} < 2$.

6. Definition of cross sections and systematic uncertainties

The ϕ-meson cross sections were measured in the kinematic region $10 < Q^2 < 100$ GeV^2, $2 \times 10^{-4} < x < 10^{-2}$, $1.7 < p_T^{\phi} < 7$ GeV and $-1.7 < \eta^{\phi} < 1.6$. The cross sections as a function of a given observable, Y, were determined from

$$\frac{d\sigma}{dY} = \frac{N}{A \cdot \mathcal{L} \cdot B \cdot \Delta Y},$$

where N is the number of events with a ϕ-meson candidate in a bin of size ΔY, A is the correction factor (which takes into account migrations, efficiencies and radiative effects for that bin) and $\mathcal{L}$ is the integrated luminosity. The branching ratio, B, for the decay channel $\phi \to K^+K^-$ was taken to be $0.492^{+0.006}_{-0.007}$ [18].

The acceptance for each kinematic bin was calculated as $\mathcal{A}^{\text{rec}}/\mathcal{A}^{\text{gen}}$, where $\mathcal{A}^{\text{rec}}$ ($\mathcal{A}^{\text{gen}}$) is the reconstructed (generated) number of events with ϕ mesons. For the calculation of the acceptance, 2.7% of the total number of inclusive DIS events generated with ARIADNE were replaced by diffractive events from PYTHIA. While the contribution from diffractive ϕ-meson events is negligible for the full phase-space region, it is important for the high x_p region in the Breit frame, since 72% of the diffractive ϕ-meson events have $x_p > 0.8$.

The systematic uncertainties of the measured cross sections were estimated from the following (the typical contribution from each item to the uncertainty of the total cross section is indicated in parentheses):

- event reconstruction and selection. Systematic checks were performed by changing the cuts on y_e, y_{JB}, δ and the vertex-position requirement: $y_e \leqslant 0.90$ (-0.1%), $y_{\text{JB}} > 0.05$ (-0.05%), $42 \leqslant \delta \leqslant 58$ GeV (-0.3%), $|Z_{\text{vertex}}| < 45$ cm ($+0.4\%$). The radius cut for the position of the scattered positron in the calorimeter was raised by 1 cm (-0.5%). The minimum accepted energy of the scattered positron was increased by 1 GeV (-0.1%). The positron energy scale was changed within its $\pm 2\%$ uncertainty ($^{+0.1}_{+0.7}\%$);
- the DA method was used to reconstruct the Breit frame ($+0.3\%$) and the kinematic variables ($+0.08\%$);
- the minimum transverse momentum for K-meson candidates was raised by 100 MeV ($+0.6\%$). Tracks were required to have $|\eta| < 1.75$, in addition to the requirement of three CTD superlayers ($+0.02\%$);
- the form of the background in the fits was changed to a second-order polynomial function ($+0.4\%$);
- the fraction of diffractive ϕ-meson events in the Monte Carlo sample was varied in the range 1.9–3.5% ($\pm 0.03\%$).

The overall systematic uncertainty for the differential cross sections was determined by adding the

above uncertainties in quadrature. The normalisation uncertainty due to that of the luminosity measurement, which is 1.6%, was only added to the overall systematic uncertainty for the total ϕ-meson cross section. The uncertainty in the $\phi \to K^+K^-$ decay branching ratio was not included.

7. Results

The overall ϕ-meson acceptance for $10 < Q^2 < 100$ GeV^2, $2 \times 10^{-4} < x < 10^{-2}$, $1.7 < p_T^\phi < 7$ GeV and $-1.7 < \eta^\phi < 1.6$, estimated with DJANGOH, was 45%. The total ϕ-meson cross section in this region is

$$\sigma\left(e^+ p \to e^+ \phi X\right) = 0.507 \pm 0.022(\text{stat.})^{+0.010}_{-0.008}(\text{syst.}) \text{ nb}.$$

This cross section is lower than that predicted by the LEPTO (0.680 nb) and ARIADNE (0.701 nb) models with the CTEQ5D structure function and with the LEP default value of the strangeness-suppression factor, $\lambda_s = 0.3$. The HERWIG 6.2 model for neutral current DIS processes underestimates the measured ϕ-meson cross section, predicting 0.36 nb.

In previous studies of neutral kaons and Λ baryons at HERA [6,7,23], it was found that decreasing λ_s from its standard value improved the agreement between the Lund MC models and the data. A smaller value of the strangeness-suppression factor, $\lambda_s = 0.22$, resulted in an inclusive ϕ-meson cross section of 0.501 (0.509) nb for LEPTO (ARIADNE), which agrees well with the present measurement. Therefore, $\lambda_s = 0.22$ was used as the default for LEPTO and ARIADNE in the following comparisons. A comparison of the data with the predicted cross sections gave an uncertainty of ± 0.02 on the λ_s value used in this analysis.

7.1. Differential ϕ-meson cross sections

Fig. 3 shows the differential cross sections as a function of p_T^ϕ, η^ϕ, x_p and Q^2 compared to the LEPTO, ARIADNE and HERWIG models using the CTEQ5D parton distribution functions.[54] The measured cross sections are compiled in Table 1(a)–(e). The x_p cross sections are shown separately for the current and the target regions. The ϕ-meson cross sections in the current and the target regions of the Breit frame are distinctly different: the data are concentrated at x_p around ~ 0.5 in the current region, and at ~ 1 in the target region.

The MC models based on the Lund fragmentation with $\lambda_s = 0.22$ reasonably well reproduce the p_T^ϕ and Q^2 distributions. Significant differences exist for the distributions of η^ϕ in the laboratory frame and x_p in the current region of the Breit frame. In the target region, the MC models underestimate the cross sections. If $\lambda_s = 0.3$ is used, the MC models based on the string fragmentation agree well with the data in the target region, but significantly overestimate the cross sections in the current region.

In addition to varying the λ_s values, different methods to tune the Lund MC models were considered, all of which had a negligible effect on the LEPTO predictions. In particular, the contribution to the ϕ cross section from charm events, mainly due to D and D_s decays, was investigated using AROMA [32]. This model produces charm quarks exclusively through the BGF mechanism, and reproduces the measured $D^{*\pm}$ cross sections in DIS [33]. According to AROMA, charm decays account for 20% of the ϕ mesons, contributing mainly in the target hemisphere. This fraction is larger than that predicted by LEPTO, but it is not sufficient to explain the observed discrepancies. For leading ϕ mesons ($x_p > 0.8$) in the current region, charm events give a negligible contribution.

In order to disentangle the different contributions to the ϕ-meson production and to investigate the observed discrepancies, the MC samples were divided into a few subsamples. Fig. 3 illustrates the contributions of QPM/QCDC interactions on an s or $\bar{s}$ quark of the proton sea. In this case, a struck s or $\bar{s}$ quark produces a ϕ meson after the hadronisation process. The ϕ-meson cross section in the current region of the Breit frame contains a significant fraction of events produced by hard scatterings of the virtual photon on the strange sea. This fraction rises with increasing p_T^ϕ and x_p values, while the contribution to ϕ-meson production from strange quarks produced solely in the hadronisation process becomes negligible

[54] The leading-order set, CTEQ5L, gave very similar results.

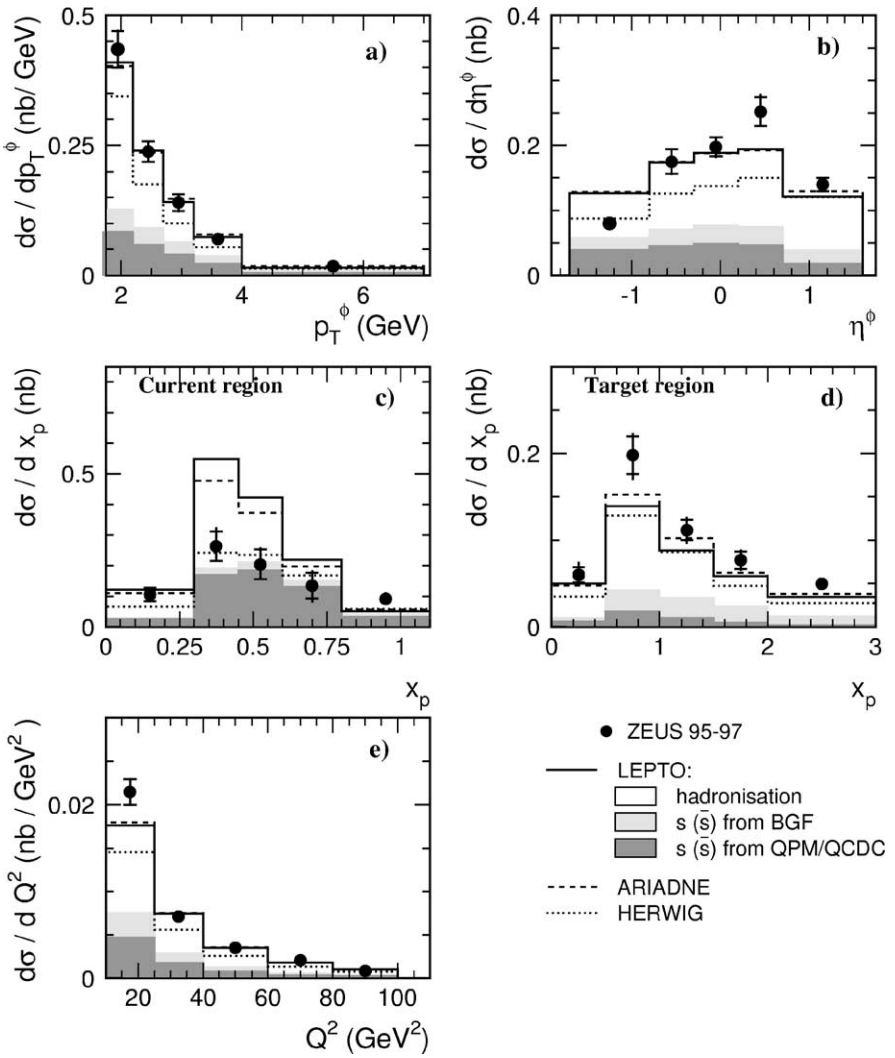

Fig. 3. Differential ϕ-meson cross sections as functions of (a) p_T^{ϕ}, (b) η^{ϕ}, (c), (d) x_p and (e) Q^2, compared to LEPTO, ARIADNE and HERWIG. The LEPTO and ARIADNE predictions are shown for $\lambda_s = 0.22$. The data are also compared to contributions from LEPTO events with ϕ mesons produced in hard interactions (s or $\bar{s}$ from BGF (light shaded area), from QPM/QCDC (dark shaded area)) and from events without strange quarks at the parton level (unshaded area). The full error bars include the systematic uncertainties, which are typically negligible compared to the statistical errors.

for $x_p > 0.8$. In contrast, the target region contains a small contribution from the QPM/QCDC events, since the second s or $\bar{s}$ from an $s\bar{s}$ pair participating in the interaction usually escapes undetected in the very forward region.

Fig. 3 also indicates the contribution of BGF processes in which the flavour of the produced quark is s or $\bar{s}$. The fraction of these BGF events is larger in the target region than in the current region.

7.2. The ϕ-meson cross section as a function of x

Production of ϕ mesons was investigated as a function of x. The s-quark density increases with decreasing x; however, the BGF contribution also increases with decreasing x due to the rise of the gluon density. Thus, the ϕ-meson cross section as a function of x depends on both the strange sea and the gluon density.

Table 1
Differential ϕ-meson cross sections as functions of p_T^ϕ, η^ϕ, Q^2 and x_p. The statistical and asymmetric systematic uncertainties are shown separately

(a) Range (GeV)	$d\sigma/dp_T^\phi$ (nb/GeV)	(b) Range	$d\sigma/d\eta^\phi$ (nb)
1.7–2.2	$0.433 \pm 0.035^{+0.014}_{-0.001}$	(-1.70)–(-0.80)	$0.079 \pm 0.009^{+0.002}_{-0.004}$
2.2–2.7	$0.237 \pm 0.019^{+0.002}_{-0.007}$	(-0.80)–(-0.30)	$0.175 \pm 0.019^{+0.002}_{-0.007}$
2.7–3.2	$0.142 \pm 0.016^{+0.002}_{-0.010}$	(-0.30)–0.20	$0.199 \pm 0.014^{+0.003}_{-0.007}$
3.2–4.0	$0.071 \pm 0.009^{+0.004}_{-0.001}$	0.20–0.70	$0.248 \pm 0.022^{+0.020}_{-0.001}$
4.0–7.0	$0.018 \pm 0.002^{+0.001}_{-0.002}$	0.70–1.60	$0.140 \pm 0.010^{+0.001}_{-0.003}$
(c) Range (GeV^2)	$d\sigma/dQ^2$ (nb/GeV^2)	(d) Range	$d\sigma/dx_p$ (target) (nb)
10–25	$0.02140 \pm 0.00148^{+0.00024}_{-0.00031}$	0.0–0.5	$0.059 \pm 0.009^{+0.013}_{-0.007}$
25–40	$0.00708 \pm 0.00047^{+0.00019}_{-0.00002}$	0.5–1.0	$0.193 \pm 0.021^{+0.031}_{-0.034}$
40–60	$0.00350 \pm 0.00040^{+0.00008}_{-0.00001}$	1.0–1.5	$0.112 \pm 0.012^{+0.006}_{-0.012}$
60–80	$0.00199 \pm 0.00026^{+0.00021}_{-0.00004}$	1.5–2.0	$0.077 \pm 0.010^{+0.008}_{-0.007}$
80–100	$0.00079 \pm 0.00021^{+0.00001}_{-0.00008}$	2.0–3.0	$0.049 \pm 0.006^{+0.004}_{-0.004}$
(e) Range	$d\sigma/dx_p$ (current) (nb)	(f) Range ($\eta_{\max} > 2$)	$d\sigma/dx_p$ (current) (nb)
0.00–0.30	$0.105 \pm 0.022^{+0.008}_{-0.001}$	0.00–0.30	$0.105 \pm 0.022^{+0.008}_{-0.001}$
0.30–0.45	$0.263 \pm 0.048^{+0.040}_{-0.006}$	0.30–0.45	$0.262 \pm 0.048^{+0.040}_{-0.006}$
0.45–0.60	$0.203 \pm 0.049^{+0.028}_{-0.018}$	0.45–0.60	$0.201 \pm 0.048^{+0.028}_{-0.018}$
0.60–0.80	$0.135 \pm 0.042^{+0.026}_{-0.036}$	0.60–0.80	$0.121 \pm 0.037^{+0.026}_{-0.035}$
0.80–1.10	$0.090 \pm 0.014^{+0.017}_{-0.015}$	0.80–1.10	$0.072 \pm 0.011^{+0.016}_{-0.015}$

The differential cross sections as a function of x for two Q^2 regions, $10 < Q^2 < 35$ GeV^2 and $35 < Q^2 < 100$ GeV^2, are shown in Fig. 4. Table 2 gives the values of the cross sections. The ϕ-meson differential cross section increases as x decreases down to the kinematic limit. The LEPTO and HERWIG MCs reproduce this rise. The LEPTO model shows the contributions of events in which a ϕ meson is produced after hadronisation of an s ($\bar{s}$) quark emerging from the hard interaction. The contributions from the QPM/QCDC and BGF processes rise with decreasing x due to the rise of the s-quark and the gluon density in the proton.

7.3. Leading ϕ mesons

The MC predictions for leading ϕ mesons ($x_p > 0.8$), usually corresponding to high p_T^ϕ in the laboratory frame, have small uncertainties both in the simulation of the QCD processes and in the hadronisation mechanism; for a given strange-sea density, the scattering of the virtual photon on a strange quark is described by the QED process, $\gamma^* s \to s$. Any additional gluon emissions are not important for $x_p > 0.8$, since such processes lead to strange quarks with smaller x_p.

Fig. 5 and Table 1(f) show the cross sections for three x_p bins in the current region of the Breit frame for the full Q^2 range, after removing the diffractive contribution with $\eta_{\max} < 2$. The hatched bands represent uncertainties in the simulation of the ϕ-meson production by the MC models LEPTO, ARIADNE and HERWIG. The uncertainty due to λ_s values between 0.2 and 0.3 is also included, such that the upper bounds of the hatched area for $x_p < 0.8$ correspond to LEPTO with $\lambda_s = 0.3$, while the lower bounds of this area indicate the HERWIG predictions.

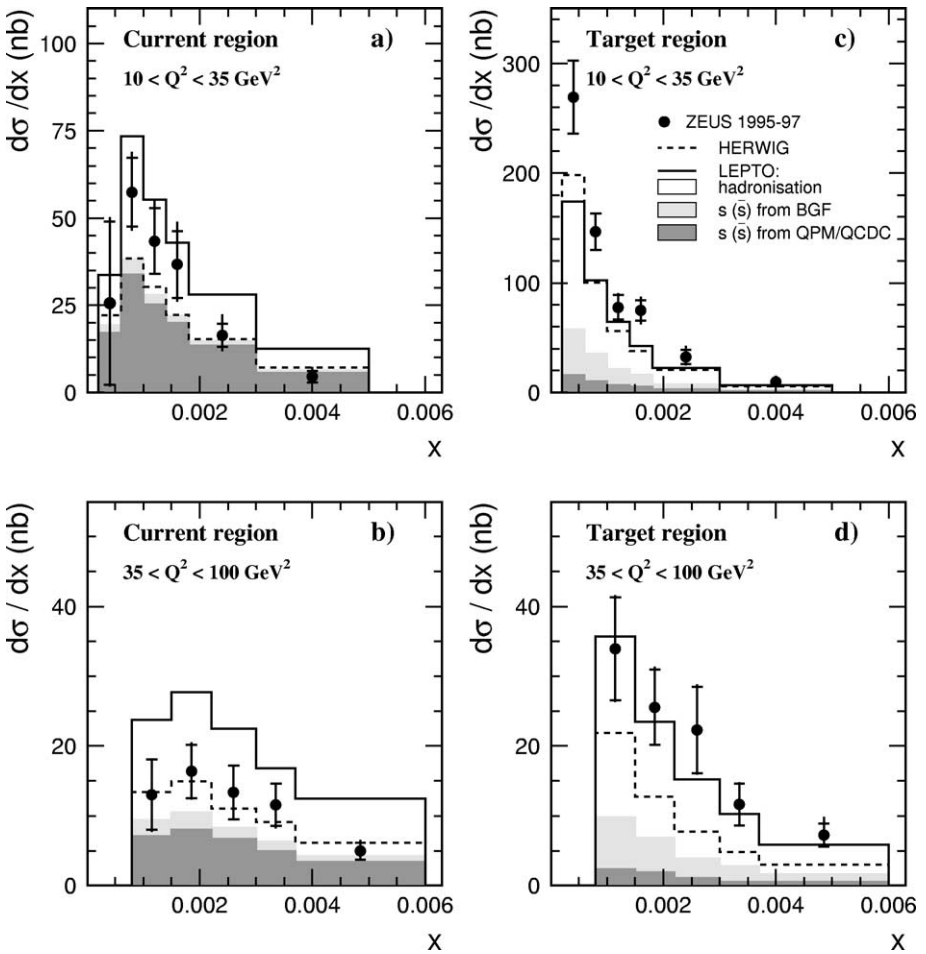

Fig. 4. The inclusive sections as a function of x for two Q^2 intervals, for the current, (a), (b), and the target, (c), (d), regions of the Breit frame compared to the HERWIG (dashed lines) and the LEPTO (solid lines) predictions with $\lambda_s = 0.22$. The LEPTO model shows separately the contributions from events with ϕ mesons produced in hard interactions (s or $\bar{s}$ from BGF (light shaded area), from QPM/QCDC (dark shaded area)) and from events without strange quarks at the parton level (unshaded area).

For $x_p > 0.8$, the HERWIG prediction is between LEPTO with $\lambda_s = 0.2$ and $\lambda_s = 0.3$. The predicted cross sections of ARIADNE are always within the shaded bands.

The MC uncertainties are small for $x_p > 0.8$. The predictions are shown with and without the contribution from the process of Fig. 1(a). The measured cross section clearly requires a contribution from interactions with the strange sea. The MCs with the CTEQ5D or the MRST99(c-g) [2] (not shown) parton distribution functions reproduce the measured rate of ϕ mesons. In these parameterisations, the strange sea is suppressed with respect to the non-strange sea, with the ratio $s\bar{s}/d\bar{d}$ in the range 0.25–0.5, depending on x. The predictions correctly describe the results and thus confirm the strange-quark suppression, even though the Q^2 values of this data are significantly larger than the strange-quark mass.

8. Conclusions

Inclusive ϕ-meson cross sections have been measured in deep inelastic scattering for $10 < Q^2 < 100$ GeV^2, $2 \times 10^{-4} < x < 10^{-2}$, $1.7 < p_T^{\phi} < 7$ GeV and $-1.7 < \eta^{\phi} < 1.6$. The MC predictions with a

Table 2
Differential ϕ-meson cross sections as a function of x for two intervals in Q^2. The statistical and asymmetric systematic uncertainties are shown separately

$10 < Q^2 < 35$ GeV^2

Range (all regions)	$d\sigma/dx$ (nb)
0.0002–0.0006	$288.6 \pm 33.0^{+7.5}_{-20.8}$
0.0006–0.0010	$216.7 \pm 24.8^{+4.6}_{-0.5}$
0.0010–0.0014	$110.0 \pm 8.5^{+5.6}_{-3.0}$
0.0014–0.0018	$105.7 \pm 17.3^{+1.9}_{-4.9}$
0.0018–0.0030	$47.8 \pm 5.3^{+0.8}_{-3.1}$
0.0030–0.0050	$11.7 \pm 3.1^{+0.9}_{-0.1}$

Current region

Range	$d\sigma/dx$ (nb)
0.0002–0.0006	$25.6 \pm 23.4^{+7.6}_{-4.7}$
0.0006–0.0010	$57.4 \pm 9.9^{+5.9}_{-5.2}$
0.0010–0.0014	$43.4 \pm 9.4^{+6.6}_{-0.3}$
0.0014–0.0018	$36.7 \pm 9.5^{+7.7}_{-4.7}$
0.0018–0.0030	$16.4 \pm 3.3^{+5.0}_{-3.0}$
0.0030–0.0050	$4.5 \pm 1.7^{+2.2}_{-0.7}$

Target region

Range	$d\sigma/dx$ (nb)
0.0002–0.0006	$269.0 \pm 33.4^{+2.8}_{-4.7}$
0.0006–0.0010	$146.1 \pm 16.6^{+0.5}_{-4.7}$
0.0010–0.0014	$78.5 \pm 11.3^{+6.9}_{-0.7}$
0.0014–0.0018	$74.7 \pm 9.2^{+8.9}_{-9.2}$
0.0018–0.0030	$32.4 \pm 6.6^{+7.5}_{-4.9}$
0.0030–0.0050	$9.4 \pm 5.2^{+4.8}_{-2.6}$

$35 < Q^2 < 100$ GeV^2

Range (all regions)	$d\sigma/dx$ (nb)
0.0008–0.0015	$45.9 \pm 13.0^{+0.5}_{-2.9}$
0.0015–0.0022	$39.0 \pm 4.6^{+1.7}_{-0.1}$
0.0022–0.0030	$36.0 \pm 8.2^{+0.8}_{-0.1}$
0.0030–0.0037	$22.0 \pm 3.4^{+0.4}_{-5.6}$
0.0037–0.0060	$10.0 \pm 1.8^{+0.2}_{-0.1}$

Current region

Range	$d\sigma/dx$ (nb)
0.0008–0.0015	$13.0 \pm 5.1^{+1.0}_{-1.6}$
0.0015–0.0022	$16.4 \pm 3.8^{+1.6}_{-1.3}$
0.0022–0.0030	$13.4 \pm 3.8^{+0.9}_{-1.1}$
0.0030–0.0037	$11.5 \pm 3.0^{+0.6}_{-1.4}$
0.0037–0.0060	$4.9 \pm 1.2^{+1.0}_{-0.7}$

Target region

Range	$d\sigma/dx$ (nb)
0.0008–0.0015	$34.3 \pm 7.5^{+2.2}_{-2.1}$
0.0015–0.0022	$25.7 \pm 5.4^{+1.2}_{-1.2}$
0.0022–0.0030	$22.2 \pm 6.2^{+2.1}_{-1.4}$
0.0030–0.0037	$11.7 \pm 3.0^{+0.9}_{-0.7}$
0.0037–0.0060	$7.2 \pm 1.7^{+2.0}_{-0.1}$

strangeness-suppression factor $\lambda_s = 0.3$ overestimate the measured cross sections. A smaller value of the strangeness-suppression factor, $\lambda_s = 0.22 \pm 0.02$, reduces the predicted cross sections and gives a good description of the total ϕ-meson cross section, as well as of the differential p_T^ϕ, Q^2 and x cross sections. However, Monte Carlo models based on Lund fragmentation fail to describe the η^ϕ and the x_p cross sections. The HERWIG simulation describes the measured cross section in the current region well, but predicts a smaller overall cross section than that measured; ϕ-meson production in the target region is underestimated by all MC models.

The production of ϕ mesons in the current region of the Breit frame has a significant contribution from the hard scattering of a virtual photon on the strange sea of the proton. The predictions for the rate of high-momentum ϕ mesons with large values of the scaled momentum, $x_p > 0.8$, in the current region of the Breit frame have small uncertainties, since the ϕ production

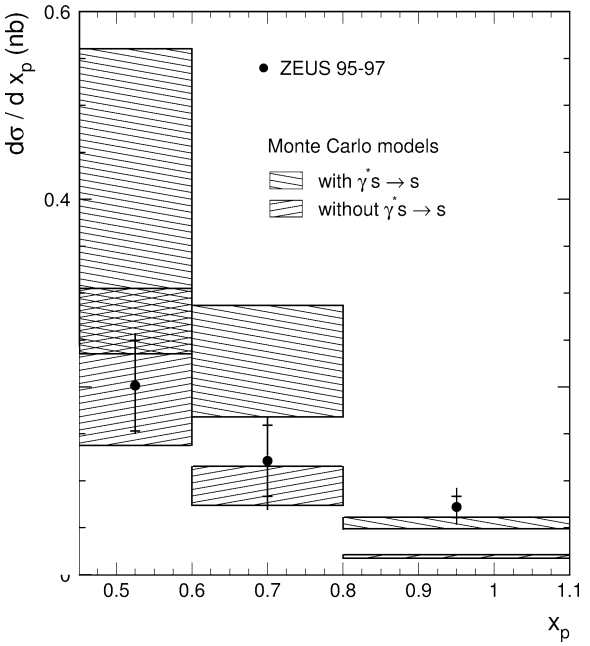

Fig. 5. The cross sections for leading ϕ mesons as a function of x_p in the current region of the Breit frame for $\eta_{\max} > 2$. The hatched bands represent uncertainties in the simulation of the ϕ-meson production by Monte Carlo models, and include LEPTO ($\lambda_s = 0.2$–0.3), ARIADNE and HERWIG. The upper bounds of the hatched area correspond to LEPTO with $\lambda_s = 0.3$, while the lower bounds of this area are defined by the LEPTO ($\lambda_s = 0.2$) and HERWIG predictions (see text).

in this region is dominated by $\gamma^* s \to s$ scattering. To reproduce the observed rate of ϕ mesons at high x_p, the MC models require a significant contribution from the strange sea of the proton. In this region, the measured cross section is correctly reproduced by these models when $\gamma^* s \to s$ scattering is included. These results constitute the first direct evidence for the existence of the strange sea in the proton at $x < 0.006$.

Acknowledgements

We thank the DESY Directorate for their strong support and encouragement. The remarkable achievements of the HERA machine group were essential for the successful completion of this work and are greatly appreciated. We are grateful for the support of the DESY computing and network services. The design, construction and installation of the ZEUS detector have been made possible owing to the ingenuity and effort of many people from DESY and home institutes who are not listed as authors.

References

[1] CTEQ Collaboration, H.L. Lai, et al., Eur. Phys. J. C 12 (2000) 375;
J. Pumplin, et al., hep-ph/0201195.
[2] A.D. Martin, et al., Eur. Phys. J. C 4 (1998) 463.
[3] M. Glück, E. Reya, A. Vogt, Eur. Phys. J. C 5 (1998) 461.
[4] H1 Collaboration, C. Adloff, et al., Eur. Phys. J. C 21 (2001) 33;
ZEUS Collaboration, S. Chekanov, et al., Phys. Rev. D, in press, DESY-02-105.
[5] CCFR Collaboration, A.O. Bazarko, et al., Z. Phys. C 65 (1995) 189;
NuTeV Collaboration, M. Goncharov, et al., Phys. Rev. D 64 (2001) 112006;
NuTeV Collaboration, T. Adams, et al., in: J.A. Gracey, T. Greenshaw (Eds.), 8th International Workshop on Deep Inelastic Scattering and QCD (DIS00), World Scientific, Singapore, 2001, p. 93.
[6] ZEUS Collaboration, M. Derrick, et al., Z. Phys. C 68 (1995) 29.
[7] H1 Collaboration, S. Aid, et al., Nucl. Phys. B 480 (1996) 3.
[8] R.P. Feynman, Photon–Hadron Interactions, Benjamin, New York, 1972;
K.H. Streng, T.F. Walsh, P.M. Zerwas, Z. Phys. C 2 (1979) 237.
[9] ZEUS Collaboration, U. Holm (Ed.), The ZEUS Detector, Status Report (unpublished), DESY (1993), available on http://www-zeus.desy.de/bluebook/bluebook.html.
[10] N. Harnew, et al., Nucl. Instrum. Methods A 279 (1989) 290;
B. Foster, et al., Nucl. Phys. (Proc. Suppl.) B 32 (1993) 181;
B. Foster, et al., Nucl. Instrum. Methods A 338 (1994) 254.
[11] M. Derrick, et al., Nucl. Instrum. Methods A 309 (1991) 77;
A. Andresen, et al., Nucl. Instrum. Methods A 309 (1991) 101;
A. Caldwell, et al., Nucl. Instrum. Methods A 321 (1992) 356;
A. Bernstein, et al., Nucl. Instrum. Methods A 336 (1993) 23.
[12] A. Bamberger, et al., Nucl. Instrum. Methods A 401 (1997) 63.
[13] ZEUS Collaboration, S. Chekanov, et al., Eur. Phys. J. C 21 (2001) 443.
[14] A. Bamberger, et al., Nucl. Instrum. Methods A 382 (1996) 419.
[15] H. Abramowicz, A. Caldwell, R. Sinkus, Nucl. Instrum. Methods A 365 (1995) 508.
[16] S. Bentvelsen, J. Engelen, P. Kooijman, in: W. Buchmüller, G. Ingelman (Eds.), Proc. Workshop on Physics at HERA, Vol. 1, DESY, Hamburg, Germany, 1992, p. 23;
K.C. Höger, in: W. Buchmüller, G. Ingelman (Eds.), Proc. Workshop on Physics at HERA, Vol. 1, DESY, Hamburg, Germany, 1992, p. 43.
[17] F. Jacquet, A. Blondel, in: U. Amaldi (Ed.), Proceedings of the Study for an *ep* Facility for Europe, Hamburg, Germany, 1979, p. 391, also in preprint DESY 79/48.

[18] Particle Data Group, K. Hagiwara, et al., Phys. Rev. D 66 (2002) 010001.
[19] B. Andersson, et al., Phys. Rep. 97 (1983) 31.
[20] OPAL Collaboration, P.D. Acton, et al., Z. Phys. C 56 (1992) 521;
OPAL Collaboration, R. Akers, et al., Z. Phys. C 68 (1995) 1;
ALEPH Collaboration, D. Buskulic, et al., Z. Phys. C 69 (1996) 379;
DELPHI Collaboration, P. Abreu, et al., Z. Phys. C 73 (1996) 61.
[21] OPAL Collaboration, G. Abbiendi, et al., Eur. Phys. J. C 16 (2000) 407.
[22] SLD Collaboration, K. Abe, et al., Phys. Rev. D 59 (1999) 052001.
[23] ZEUS Collaboration, J. Breitweg, et al., Eur. Phys. J. C 2 (1998) 77.
[24] G. Ingelman, A. Edin, J. Rathsman, Comput. Phys. Commun. 101 (1997) 108.
[25] L. Lönnblad, Comput. Phys. Commun. 71 (1992) 15.
[26] G. Marchesini, et al., Comput. Phys. Commun. 67 (1992) 465.
[27] T. Sjöstrand, Comput. Phys. Commun. 82 (1994) 74.
[28] B.R. Webber, Nucl. Phys. B 238 (1984) 492;
G. Marchesini, B.R. Webber, Nucl. Phys. B 310 (1988) 461.
[29] A. Kwiatkowski, H. Spiesberger, H.-J. Möhring, Comput. Phys. Commun. 69 (1992) 155, also in: Proc. Workshop Physics at HERA, DESY, Hamburg, 1991.
[30] H. Spiesberger, HERACLES and DJANGOH: Event Generation for *ep* Interactions at HERA Including Radiative Processes, 1998, available on http://www.desy.de/~hspiesb/djangoh.html.
[31] R. Brun, et al., GEANT3, Technical Report CERN-DD/EE/84-1, CERN, 1987.
[32] G. Ingelman, J. Rathsman, G.A. Schuler, Comput. Phys. Commun. 101 (1997) 135.
[33] H1 Collaboration, C. Adloff, et al., Z. Phys. C 72 (1996) 593;
ZEUS Collaboration, J. Breitweg, et al., Eur. Phys. J. C 12 (2000) 35;
H1 Collaboration, C. Adloff, et al., Phys. Lett. B 528 (2002) 199.